Large-eddy simulation of idealized hurricanes at different sea surface temperatures

Hehe Ren[1], Jimy Dudhia[2], and Hui Li[1]

[1]Harbin Institute of Technology
[2]National Center for Atmospheric Research (UCAR)

November 21, 2022

Abstract

Idealized hurricanes are studied at four different sea surface temperatures (ssts) of 26°, 27°, 28°, and 29°C in six nested domains down to 62 m grid size. For the maximum and the distribution of wind speed, domain D6 (62 m) is similar to domain D5 (185 m) showing convergence near 200 m. For sst of 26°, domain 5 does not have small-scale turbulence structures like the other three cases, which is an extension of the previous work of [2009] who only obtained resolved gusts at 62 m. The distribution function of speed changes between the 27° and 28° cases, the latter one having a second peak, related to a structural change. Finally, it is suggested that the damage potential is not simply determined by the maximum wind speed because of the distribution change so a new damage indicator that represents potential damage is proposed.

Large-eddy simulation of idealized hurricanes at different sea surface temperatures

Hehe Ren[1,2], Jimy Dudhia[3], and Hui Li[1,2]

[1]Key Lab of Smart Prevention and Mitigation for Civil Engineering Disasters of the Ministry of Industry and Information, Harbin Institute of Technology, Harbin 150090, China.

[2]Key Lab of Structures Dynamic Behavior and Control of the Ministry of Education, Harbin Institute of Technology, Harbin, 150090, China.

[3]Mesoscale and Microscale Meteorology Laboratory, National Center for Atmospheric Research, Boulder, Colorado.

Corresponding author: Hehe Ren (renhehe@hit.edu.cn)

Key Points:

- The hurricane structure changes as sea surface temperature increases: the distribution function of wind speed changes from single peak to bimodal.
- The scale of turbulent eddies increases as sea surface temperature increases. For hurricane intensity, a horizontal grid size near 200 m is sufficient for a converged solution.
- A new damage indicator is proposed for hurricane disaster risks.

Abstract

Idealized hurricanes are studied at four different sea surface temperatures (ssts) of 26°, 27°, 28°, and 29°C in six nested domains down to 62 m grid size. For the maximum and the distribution of wind speed, domain D6 (62 m) is similar to domain D5 (185 m) showing convergence near 200 m. For sst of 26°, domain 5 does not have small-scale turbulence structures like the other three cases, which is an extension of the previous work of *Rotunno et al.* [2009] who only obtained resolved gusts at 62 m. The distribution function of speed changes between the 27° and 28° cases, the latter one having a second peak, related to a structural change. Finally, it is suggested that the damage potential is not simply determined by the maximum wind speed because of the distribution change so a new damage indicator that represents potential damage is proposed.

Plain Language Summary

The warm sea surface greater than 26°C contributes to the formation and development of hurricanes. In addition, the hurricane strength and structure are very sensitive differences in sea surface temperature that will lead to different degrees of disaster impact on coastal areas. Here we focus on how wind speeds are distributed in high-resolution simulations with grids down to 62 m at sea-surface temperatures of 26-29°C that resolve the damaging gusts. Standard maximum wind measures (such as hurricane category) are found to be inadequate in some cases because they do not account for area. Integrated functions of wind speed from these simulations are then proposed as improved measures of potential damage.

1 Introduction

High resolution simulation is necessary for detailed hurricane research, because some turbulence structures do not become resolved until a hundred meters or ten meters resolution is used. These turbulence structures will be the source of damage to offshore structures, such as wind farms and oil rigs, and coastal buildings [*Worsnop et al.,* 2017a; *Worsnop et al.,* 2017b; *Bryan et al.,* 2017; *Stern and Bryan,* 2018]. *Rotunno et al.* [2009] showed that the maximum wind speed in their tropical cyclone simulation showed a strong relation with the resolved three-dimensional turbulence structure scale. However, the critical resolution is still not clear for turbulence and nonturbulence structures of hurricanes. *Rotunno et al.* [2009] found that a transition to randomly distributed, small-scale turbulent eddies occurs when the grid size decreases from 185 to 62 m at a sea surface temperature (sst) of 26.3°. In this study, we further investigate the influence of sst on hurricane intensity and turbulence structure through high resolution simulations of hurricanes at various ssts in no-shear conditions.

2 Simulation settings

The numerical simulations conducted here were carried out with the WRF model (Weather Research and Forecasting Model) [*Skamarock et al.,* 2008]. WRF adopts nonhydrostatic dynamics, and thus it can capture small-scale turbulence structures when using the WRF-LES mode. Six nested domains were used at grid sizes from 15 km to 62 m (Table 1) as in *Rotunno et al.* [2009]. The model thermodynamic state is maintained by inclusion of a relaxation term in the thermodynamic equation with a time constant of 12 h. Atmospheric radiation is one of the effects that is simply represented in the relaxation term, so no other radiative scheme was used. The cloud physics scheme is the WRF Single-Moment 6-Class scheme [WSM6, *Hong and Lim,* 2006] and the PBL mixing is handled by the YSU scheme [*Hong et al.*, 2006] in the outer three domains. The Revised MM5 Monin-Obukhov surface layer scheme [*Jimenez et al.,* 2012] was adopted, and cumulus parameterization is not considered even in the outermost 15 km domain because the hurricane is contained within the nests. Another important point is that the air-sea exchange of heat and momentum are represented by using Donelan Cd plus constant z0q method for Ck [*Donelan et al.,* 2004]. For domains D1-D3, the PBL is represented by the YSU scheme that relates the amount of vertical mixing to the stability of the PBL and surface buoyancy flux, and horizontal mixing is related to the local horizontal wind deformation. This separation of vertical and horizontal turbulence process is typical in mesoscale models. While for domains D4-D6, effects of horizontal and vertical turbulence processes are unified and parameterized using a grid-spacing-dependent eddy viscosity based on a three-dimensional turbulence-kinetic-energy equation appropriate for LES [*Deardorff,* 1980].

The initial velocity field represents an incipient TC-like axisymmetric vortex with a maximum lowest-level wind of 15 m/s, radius of maximum wind of 82.5 km, and radius of zero wind of 412.5 km [*Rotunno and Emanuel,* 1987]. The Coriolis parameter is spatially uniform with its value at 20° latitude ($5\times10^{-5}s^{-1}$).

Four simulation cases were run with sea surface temperatures of 26°, 27°, 28°, 29°C, respectively. The common details of these simulations are shown in Table 1. Note that domains D4, D5, and D6 were started at later times after day 4 and their length was shorter, but long enough to reach a steady resolved state. Furthermore, in order to capture the significant characteristics of the hurricane, such as surface radial inflow, lower-level and upper-level outflow, specific vertical levels were adopted as shown in Figure S1.

Additional high-frequency surface diagnostics were output that included time averages and other statistics, e.g. at 1-minute frequency for domain D6.

Table 1. The basic WRF simulation settings

The simulated period	2007_09_01_00:00:00~2007_09_07_00:00:00 (UTC)					
Algorithm	WRF			WRF-LES		
Domain	D1	D2	D3	D4	D5	D6
Horizontal grid distance (m)	15000	5000	1666.67	555.56	185.18	61.72
Horizontal grid number	405 × 405	301 × 301	598 × 598	598 × 598	598 × 598	967 × 967
Vertical layer number	87					
Time step (s)	60	20	6.67	2.22	0.74	0.25
Start time(dd_hh)	01_00	01_00	01_00	05_00	06_00	06_18
End time(dd_hh)	07_00	07_00	07_00	07_00	07_00	06_22

3 Results

The basic wind characteristics of simulated idealized hurricanes show in Table S1.

3.1 Wind speed and sea surface pressure

As we can see from Figure 1, both the maximum of instantaneous wind speed, time-averaged wind speed and the minimum sea surface pressure of domain D3 reach a steady state after 96 h simulation. The large-eddy simulation for domain D4 starts from 96 h. Similar to *Rotunno et al.* [2009], each parent domain is also run without nesting, thus, each simulation is independent. Importantly, Figure 1 shows that the hurricane peak strength generally increases as the grid size decreases, but a significant feature is that for both the maximum of instantaneous wind speed, time-averaged wind speed, and the minimum sea surface pressure, domain D6 (62 m) converges to domain D5 (185 m), which means that for hurricane intensity, a horizontal grid size near 200 m is sufficient. Note also that the peak for sst-27° is sometimes higher than that for sst-28°.

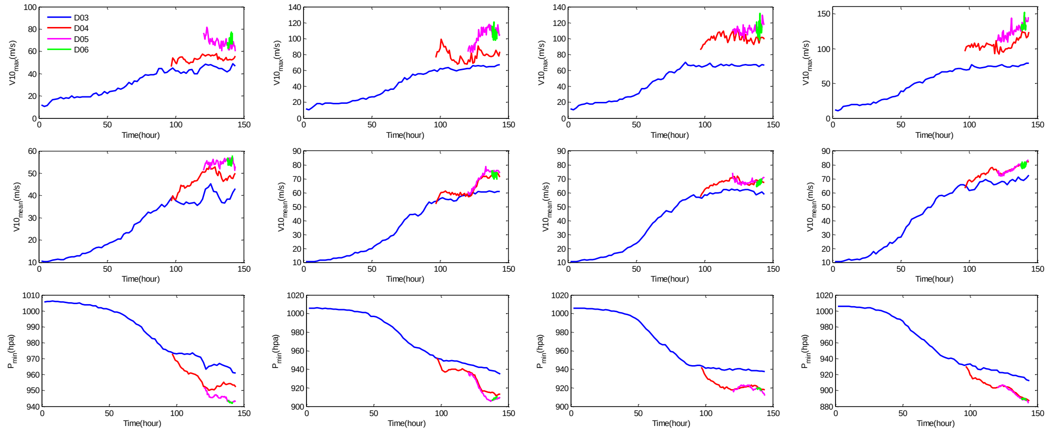

Figure 1. The maximum of instantaneous (upper), time-averaged (middle) wind speed and the minimum of sea surface pressure (bottom), subfigures represent 26°, 27°, 28°, and 29°C from left to right, respectively. Time average is 1 and 10 minutes for domains D6 and D5.

3.2 Turbulence field

Figure 2 shows the wind field of each domain of each case at the lowest model level. For sst-26° case, the features are consistent with *Rotunno et al.* [2009] of sst-26.3°, that transition to randomly distributed, small-scale turbulent eddies occurs between 185 and 62 m, while for other three cases, this transition occurs between 556 and 185 m, which means that the turbulent eddies are resolved at larger grid sizes as the sst increases. This may because with sst increases, the radial inflow depth increases (Figure S2) which means the scale of dominant vortices increases, thus, the vortex scale becomes resolvable between 556 and 185 m.

Furthermore, from the perspective of the wind velocity wavenumber spectrum, we can confirm the turbulence structure shows different characteristics for different cases similar to the turbulence field. Figure S3 shows the wavenumber spectrum of wind velocity at the height of 10 m. It is clear that for sst-26° case, only domain D6 has a -5/3 slope subregion, as we note that a -5/3 slope represents a three-dimensional turbulence structure; while for the other three cases, both domains D6 and D5 have the -5/3 slope subregion; so the features of the wavenumber spectrum agree well with the turbulence fields seen earlier. This illustrates that sst-26° has different wind characteristics from the three stronger cases, specifically that sst can influence the hurricane intensity and scale of the turbulence structures. This aspect of the study has extended the result of *Rotunno et al.* [2009].

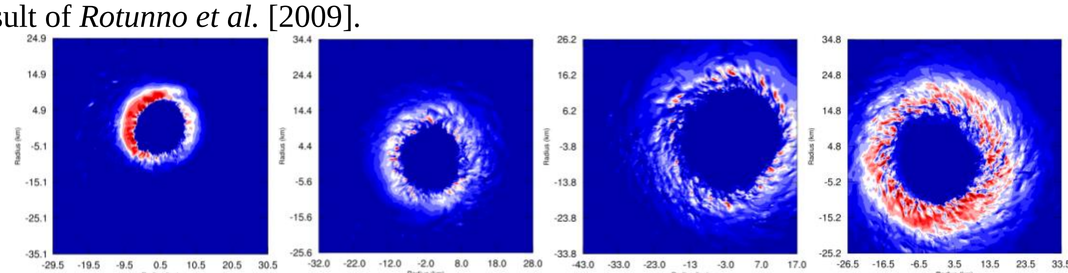

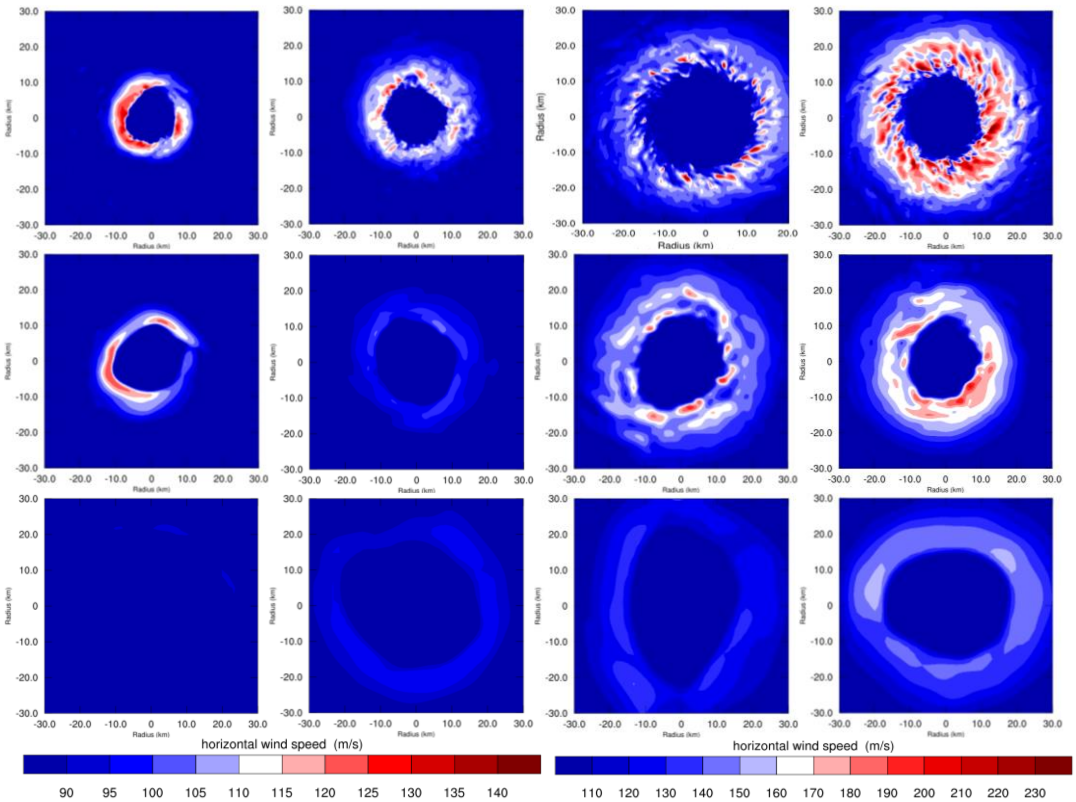

Figure 2. Wind field of each domain of each case at the lowest level. Subfigures represent 26°, 27°, 28°, and 29°C from left to right, and domains D6, D5, D4, and D3 from upper to bottom, respectively. Here, need to note that the 26°case (the left color bar) has a different unit with the other three cases (the right color bar).

3.3 Wind speed distribution

For both the maximum of instantaneous wind speed, time-averaged wind speed and minimum sea surface pressure, it is easily seen that the wind speed and pressure of case sst-27° and case sst-28° has “crossover” features as shown in Figure S4 for all the domains. The reason for this is the motivation of this section because hurricanes are often characterized by maximum wind speed, and it will become clear that this may be misleading in some cases.

Figure 3a shows the frequency distribution of wind speed for each domain of each case. Compared with the 26° and 27° cases, the 28° and 29° cases have an obvious second peak value in the distribution for domains D4, D5, and D6. In Figure 3a, it can again be seen that the largest wind speed of sst-27° is larger than sst-28°, while sst-28° has a larger wind speed area > 60 m/s, namely the second peak, meaning that from case sst-27° to case sst-28°, the wind speed distribution changes to bimodal. This can be seen in Figure 3b, which shows the radial distribution of wind speed. It is found that the physical interpretation of the second peak is that the hurricane has a wide eyewall region (a flatter peak near the radius of maximum speed), specifically, the wide peak region of Figure 3b corresponds to the second peak value of Figure 3a. For cases sst-26° and sst-27°, none of the domains have a wide eyewall region. On the contrary, for cases sst-28° and sst-29°, domains D4, D5 and D6 have wide eyewall regions which appear to need grid sizes < 1 km to exist since domain D3 (1.66km) showed no such feature. In addition, Figure 3c shows the predominant magnitude of wind speed (peak of the distribution) of each case for domain D6 (domains D4 and D5 have similar features). It is clearly seen that for cases sst-28° and sst-29°, this predominant magnitude is located in the eyewall region, while it is not for cases sst-26° and sst-27°. The two stronger cases with large eyewall radii and a more uniform strong wind in the azimuthal direction resemble annular hurricane structures that have been documented as sometimes occurring after an eyewall replacement cycle [*Knaff et al.*, 2003; *Wang*, 2008]. It should be noted again that the maximum wind may be misleading as a damage indicator given how much the relative areas of strong wind vary with sst.

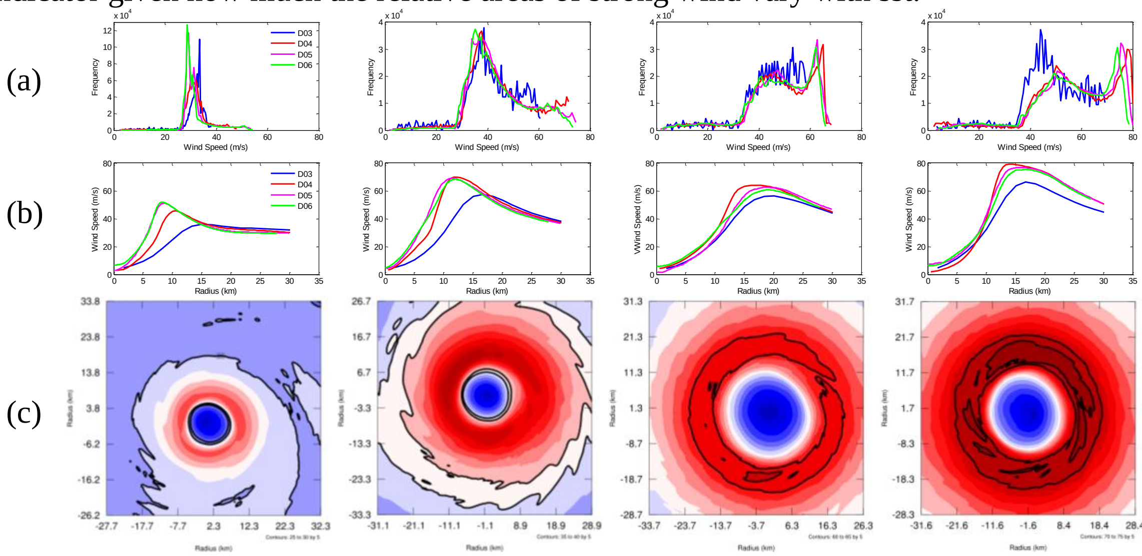

Figure 3. The histogram distribution of wind speed (a), the radial distribution of wind speed (b), and time-averaged wind field of domain D6 (c) of each case. Subfigures represent 26°, 27°, 28°, and 29°C from left to right, and for (c) between the black lines means that the predominant magnitude of wind speed, 25-30 m/s, 35-40 m/s, 60-65 m/s and 70-75 m/s for 26°, 27°, 28°, and 29°C, respectively.

4 A new potential damage indicator

Finally, since maximum wind alone may be insufficient for the damage potential, we will consider some ways to area-integrate the effect of the hurricane. The integrated kinetic energy [*Powell and Reinhold*, 2007] is defined, $IKE = \int_V 1/2\, \rho U^2 dV$, where the wind speeds are taken from each grid cell of each domain and integrated nominally 1 m in the vertical (centered at the 10 m level). Because the value becomes too sensitive to domain area when weak winds are included, a wind speed of 10 m/s was selected for the low end $IKE_{>10}$ following *Powell and Reinhold* [2007]. Detailed $IKE_{>10}$ results are shown in Table S2 as an indicator of destructive potential [*Powell and Reinhold*, 2007]. This illustrates the difference between ssts for each domain, and it is easily concluded in general that the destructive potential increases with sst increases. Also wind destructive potential thresholds are defined that include light (25 to < 41 m/s, IKE_{25-40}), moderate (41 to < 55 m/s, IKE_{41-54}), and severe (>=55 m/s, IKE_{55}), from which *Powell and Reinhold* [2007] define a damage-weighted sum as a damage indicator, $IKE_{25-40} + 6IKE_{41-54} + 30IKE_{55}$. It is clear that for the wind destructive potential sst-28° is also larger than sst-27° for each domain in Figure 5a despite the lower maximum wind described in the previous section.

Figure 3 in the *Powell and Reinhold* [2007] reproduced here in Figure 4 shows that the damage percentage (claim to insured value) is very nonlinear and almost exponential with wind speed < 60 m/s. We will therefore define three potential damage functions as $\log_{10} D = WS10/10 - 4$ (formula-1) as lower bound, $\log_{10} D = WS10/20 - 1$ (formula-2) as upper bound and $\log_{10} D = WS10/15 - 2$ (formula-3) as a median value, where D means potential damage (%), and $WS10$ means the maximum sustained wind at an elevation of 10 m. These lines are also shown in Figure 4. Here 100% damage occurs at 60 m/s for all three methods, but 1% occurs at 40 m/s, 20 m/s and 30 m/s, respectively. It is meaningful to calculate the area integral of *D* similarly to the way IKE is derived from area-integrating kinetic energy. Figure 5a shows the relationship between the integrated damage (unit, 10^{10} % m^2) (also shown in Table S3) and total wind damage-weighted IKE (unit, TJ). Here note that the area integral of *D*, which compares with the IKE, is hereafter named D_{area}. A value of $D = 10^{10}$ % m^2 is equivalent to 100% damage in a 10 km square or 1 % damage in a 100 km square and is therefore a representation of relative cost. It directly shows that the damage of sst-28° is larger than sst-27°. The larger the D_{area}, the larger the total wind damage-weighted IKE, which shows a strong linear relationship. This indicates that D_{area} is a good alternative index to represent the potential damage. Note that for different formulas of D_{area}, the small speed part has a different weight, so the value of D_{area} is sensitive to the formula because smaller velocities occupy larger areas. These three formulas may be suitable to different regions where offshore or coastal structures have different wind resistance levels according to age and building codes. Also, in Figure 5a, the D_{area} of domain D3 of each case is always smaller than other domains, while the D_{area} of domains D4, D5 and D6 are almost converged showing the importance of resolution < 1 km.

However, the area integral may not be the best measure because it underestimates the relative area affected by the strongest winds in a moving hurricane, so we will modify D to be integrated by radius taking the maximum D within that radius, named D_{radius} (unit, 10^3 % m or % km). This can be thought of as the integral along a coast as the hurricane crosses it and a value of 1000 % km corresponds to 100% damage on a 10 km coast. Figure S5 shows the radial distribution of D, which gives an intuitive picture of the damage potential at different distances from eye region. And for Figure 5b, the total wind damage-weighted IKE and D_{radius} (also shown in Table S4) shows a nonlinear relationship, which is different from the linear relationship of the total wind damage-weighted IKE and D_{area}.

Furthermore, the comparison of D_{area} and D_{radius} for total area of each case is shown in Figure 5c. It is clear that D_{area} and D_{radius} have a positive correlation. D_{area} is the area integral, which is more sensitive to outer weak winds, and D_{radius} is the radial integral emphasizing the eye where the damage may be 100%, and the contribution of outer weak wind becomes relatively smaller. Therefore, the change of D_{area} is greater than D_{radius} between different formulas for D that have different weak-wind tails. For example, for D_{area} the factor between the formulas changes by two, but for D_{radius} it only changes by around 10-20% for the sst-29° case. From this perspective, D_{radius} is more dominated by the inner hurricane region, and we conclude that D_{radius} is a much better index to weight the relative damage between storms. And in Figure 5b, formula-3 seems better than other two formulas where 1% damage corresponds wind speeds around category-1 hurricane strength (~33 m/s) which seems to be more justifiable, but as mentioned the other two formulas may be more suited to less (formula-1) or more (formula-2) vulnerable structures.

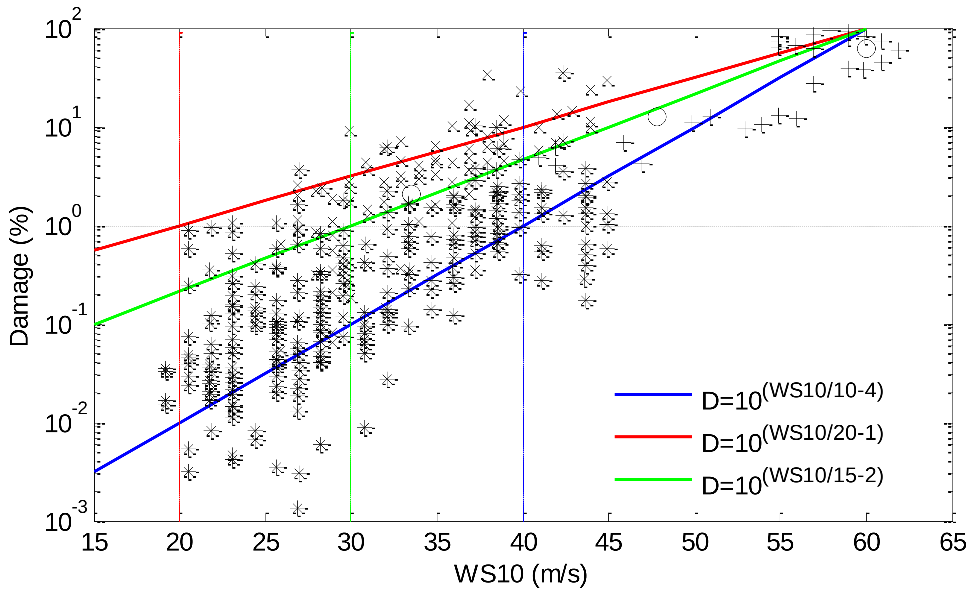

Figure 4. Wind damage as a function of $WS10$. The scatter points represent the Hurricanes Andrew, Hugo and Opal, as shown in Figure 3 of *Powell and Reinhold* [2007]. And the three solid color lines represent the three new damage indicator formulas that defined in the present study.

(a)
(b)
(c)

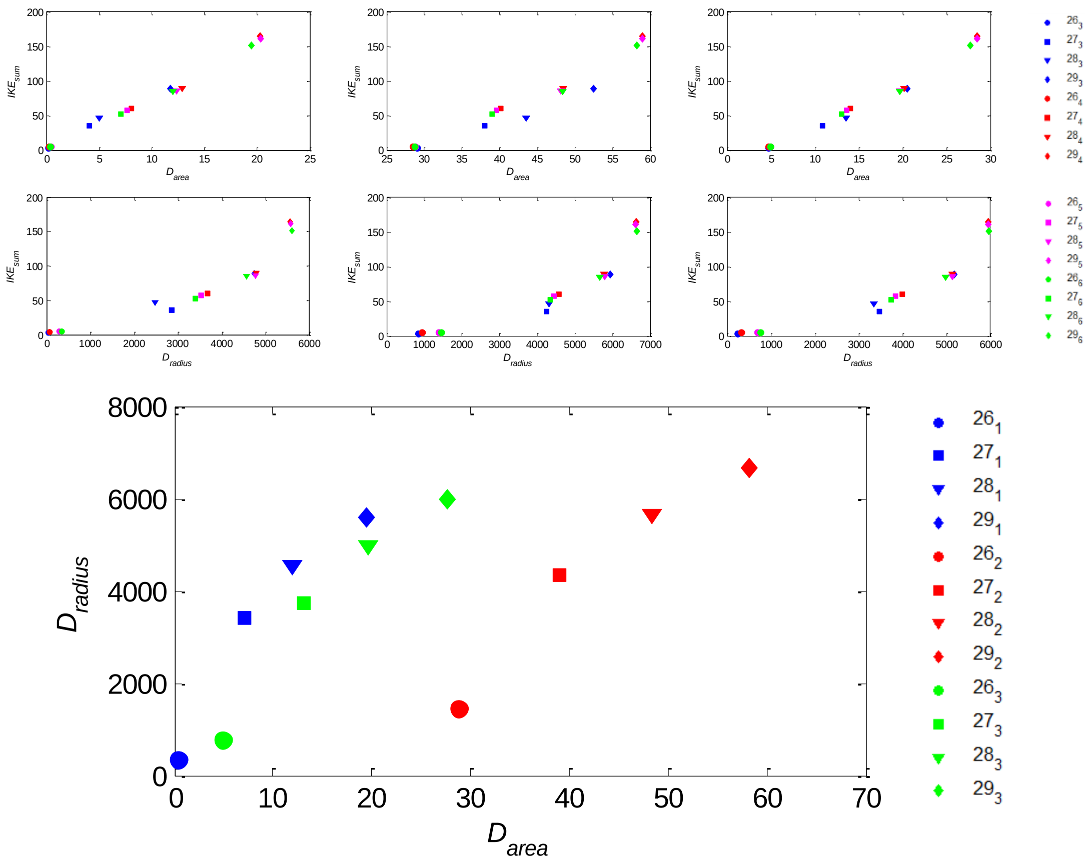

Figure 5. Comparison of Damage D_{area} (a, 10^{10} % m^2) and D_{radius} (b, 10^3 % m or % km) to total wind damage-weighted IKE, which is the sum: $IKE_{25-40} + 6IKE_{41-54} + 30IKE_{55}$. The subfigures of (a) and (b) represent wind damage calculated by formula-1,2, and 3 from left to right, respectively, and the legend in (a) and (b) shows that normal number represents the sst, and the subscript number represents the domain. (c) is the comparison of the total area D_{area} and D_{radius} for each case, and the legend in (c) shows that normal number represents the sst, and the subscript number represents the different damage indicator formulas.

5 Conclusions

In this study, we concluded that idealized hurricanes show different characteristics at different sea surface temperatures in six nested domains down to 62 m grid size. Four cases were conducted, with sea surface temperatures of 26°, 27°, 28°, 29°C, respectively. Some interesting phenomena were obtained. First, for both the maximum of instantaneous wind speed, time-averaged wind speed and the minimum sea surface pressure, domain D6 (62m) converges to the same intensity as domain D5 (185m) showing the adequacy of 185 m grid sizes. Second, for sea surface temperature of 26°, domain D5 does not have small-scale turbulence structures, but the other three cases all have, this is also an extension of the previous work of *Rotunno et al.* [2009]. Another important result is that the distribution function of speed changes between sst-27° and sst-28° case, and has different shapes between the sst-26°, sst-27° cases and the sst-28°, sst-29° cases, the latter ones having a second peak, which means that some fundamental aspect of the hurricane structure changes as sea surface temperature increases. Even though sst-27° had some higher peak wind speeds than sst-28°, the latter had broader areas of strong wind leading us to consider damage potential differences between storms that are not simply determined by the traditional maximum wind measure. Finally, three new damage indicator formulas of potential damage D and two types D_{area} and D_{radius} were introduced, all are useful damage indicators, while, D_{radius} and formula-3 seems to be the most easily justified.

Acknowledgments

This study is financially supported by the National Key Research and Development Program of China under grant No. 2018YFC0705605. NCAR is sponsored by the National Science Foundation. And, Hehe Ren thanks funding support from the China Scholarship Council (Grant No. 201806120241). We also acknowledge high-performance computing support from Cheyenne (doi:10.5065/D6RX99HX) provided by the NCAR's CISL. WRF simulation data output from this study is stored on Research Data Archive of NCAR and are available at https://rda.ucar.edu/datasets/ds301.0/.

References

Bryan, G. H., Worsnop, R. P., Lundquist, J. K., and Zhang, J. A. (2017), A simple method for simulating wind profiles in the boundary layer of tropical cyclones, Bound.-Layer Meteorol., 162(3), 475–502, doi:10.1007/s10546-016-0207-0.

Deardorff, J. W. (1980), Stratocumulus-capped mixed layers derived from a three-dimensional model, Bound.-Layer Meteorol., 18, 495–527, doi:10.1007/BF00119502.

Donelan, M. A., Haus, B. K., Reul, N., Plant, W. J., Stiassnie, M., Graber, H. C., et al. (2004), On the limiting aerodynamic roughness of the ocean in very strong winds, Geophys. Res. Lett., 31, L18306, doi:10.1029/2004GL019460.

Hong, S. Y., and Lim, J. O. J. (2006), The WRF Single-Moment 6-Class Microphysics Scheme (WSM6), J. Korean Meteor. Soc., 42, 129–151.

Hong, S. Y., Noh, Y., and Dudhia, J. (2006), A new vertical diffusion package with an explicit treatment of entrainment processes, Mon. Wea. Rev., 134, 2318–2341, doi:10.1175/MWR3199.1.

Jimenez, P. A., Dudhia, J., Gonzalez-Rouco, J. F., Navarro, J., Montavez, J. P., and Garcia-Bustamante, E. (2012), A revised scheme for the WRF surface layer formulation, Mon. Wea. Rev., 140, 898–918, doi:10.1175/MWR-D-11-00056.1.

Knaff, J. A., Kossin, J. P., and DeMaria, D. (2003), Annular hurricanes, Wea. Forecasting, 18, 204–223, doi:10.1175/1520-0434(2003)018<0204:AH>2.0.CO;2.

Powell, M. D., and Reinhold T. A. (2007), Tropical cyclone destructive potential by integrated kinetic energy, Bull. Amer. Meteor. Soc., 88, 513–526, doi:10.1175/BAMS-88-4-513.

Rotunno, R., Chen, Y., Wang, W., Davis, C., Dudhia, J., and Holland, G. J. (2009), Large-eddy simulation of an idealized tropical cyclone, Bull. Amer. Meteor. Soc., 90, 1783–1788, doi:10.1175/2009BAMS2884.I.

Rotunno R., and Emanuel K. A. (1987), An air–sea interaction theory for tropical cyclones. Part II: evolutionary study using a nonhydrostatic axisymmetric numerical model, J. Atmos. Sci., 44(3), 542–561, doi:10.1175/1520-0469(1987)044<0542:AAITFT>2.0.CO;2.

Skamarock, W. C., Klemp, J. B., Dudhia, J., Gill, D. O., Barker, D. M., Wang, W., et al. (2008), A description of the Advanced Research WRF Version 3, NCAR Tech. Note, NCAR/TN-475+STR, 113 pp.

Stern, D. P., and Bryan, G. H. (2018), Using simulated dropsondes to understand extreme updrafts and wind speeds in tropical cyclones, Mon. Weather Rev., 146, 3901–3925, doi:10.1175/MWR-D-18-0041.1.

Wang, Y. (2008), Structure and formation of annular hurricane simulated in a fully compressible, nonhydrostatic model–TCM4, J. Atmos. Sci., 65, 1505–1527, doi:10.1175/2007JAS2528.1.

Worsnop, R. P., Lundquist, J. K., Bryan, G. H., Damiani, R., and Musial, W. (2017a), Gusts and shear within hurricane eyewalls can exceed offshore wind-turbine design standards, Geophys. Res. Lett., 44, 6413–6420, doi:10.1002/2017GL073537.

Worsnop, R. P., Bryan, G. H., Lundquist, J. K., and Zhang, J. A. (2017b), Using large-eddy simulations to define spectral and coherence characteristics of the hurricane boundary layer for wind-energy applications, Bound.-Layer Meteorol., 165:55–86, doi:10.1007/s10546-017-0266-x.